













## Obrabotka metallov -

## Metal Working and Material Science

Journal homepage: [http://journals.nstu.ru/obrabotka\\_metallov](http://journals.nstu.ru/obrabotka_metallov)

## Preparation of coatings with high infrared emissivity

Vyacheslav Sirota<sup>1, a</sup>, Sergey Zaitsev<sup>1, b</sup>, Mikhail Limarenko<sup>1, c</sup>, Dmitry Prokhorenkov<sup>1, d</sup>,  
Mikhail Lebedev<sup>1, e</sup>, Anton Churikov<sup>1, f</sup>, Alexey Dan'shin<sup>2, g</sup>

<sup>1</sup> Belgorod State Technological University named after V.G. Shukhov, 46 Kostyukova st., Belgorod, 308012, Russian Federation<sup>2</sup> JSC "Shebekinsky Machine-Building Plant", 11 Oktyabrskaya st., Shebekino, 309290, Russian Federation<sup>a</sup>  <https://orcid.org/0000-0003-4634-7109>,  [zmas36@mail.ru](mailto:zmas36@mail.ru); <sup>b</sup>  <https://orcid.org/0000-0003-0122-1908>,  [sergey-za@mail.ru](mailto:sergey-za@mail.ru);<sup>c</sup>  <https://orcid.org/0000-0001-6699-6910>,  [mclam@mail.ru](mailto:mclam@mail.ru); <sup>d</sup>  <https://orcid.org/0000-0002-6455-8172>,  [bstu-cvt-sem@yandex.ru](mailto:bstu-cvt-sem@yandex.ru);<sup>e</sup>  <https://orcid.org/0000-0003-3194-9238>,  [michaell1987@yandex.ru](mailto:michaell1987@yandex.ru); <sup>f</sup>  <https://orcid.org/0000-0002-1829-2676>,  [churikov.toni@mail.ru](mailto:churikov.toni@mail.ru);<sup>g</sup>  <https://orcid.org/0009-0009-6998-8241>,  [aldans@mail.ru](mailto:aldans@mail.ru)

## ARTICLE INFO

## Article history:

Received: 13 December 2023

Revised: 26 February 2024

Accepted: 20 March 2024

Available online: 15 June 2024

## Keywords:

Detonation spraying

High emissivity coating

## Funding

The research was carried out within the framework of the Complex Project No. 30/22 dated 10/12/22 within the framework of Agreement No. 075–11-2023-017 dated 02/13/2023 "Creation of high-tech production of composite cutting elements of machines and thermal equipment for processing agricultural products".

## Acknowledgements

The research was carried out using the equipment of the Center for High Technologies of BSTU named after V.G. Shukhov.

## ABSTRACT

**Introduction.** One of the promising modern methods of coating formation is detonation gas dynamic sputtering. Coatings obtained by this method have high adhesion to the substrate, dense structure and specified functional properties. Development of technology for obtaining functional coatings with high emission coefficient in the infrared range is an urgent need for the development of high-temperature industrial processes and technologies. High-temperature industrial processes consume a large amount of energy, so improving the energy efficiency of industrial equipment is considered as one of the ways to overcome the ever-growing energy crisis. To this end, coatings with high infrared emissivity have been developed for industrial furnaces. These coatings are usually applied to the furnace walls, which significantly improves energy efficiency by increasing heat transfer from the heat-emitting surfaces of the furnace. **The purpose of the work** is to obtain coatings with high emission indices in the infrared range for further recommendation of its use in baking ovens of *Shebekinsky* machine-building plant. **Methods** for studying coating specimens obtained by detonation gas-thermal method: scanning electron microscopy, X-ray phase analysis, energy dispersive analysis, infrared spectroscopy. **Results and discussion.** The microstructure, phase composition, emissivity and thermal cycling resistance of  $Fe_2O_3$ ;  $Al_2O_3 + 10\% Fe_2O_3$ ;  $Ti + 10\% Fe_2O_3$  coatings obtained by detonation gas-dynamic powder spraying are investigated in this work. The results of the study showed that the obtained coatings have a dense structure, increased emissivity and resistance to thermal treatment cycles, as a result of which the structure of the crystal lattice of the coatings does not change.

**For citation:** Sirota V.V., Zaitsev S.V., Limarenko M.V., Prokhorenkov D.S., Lebedev M.S., Churikov A.S., Dan'shin A.L. Preparation of coatings with high infrared emissivity. *Obrabotka metallov (tekhnologiya, oborudovanie, instrumenty) = Metal Working and Material Science*, 2024, vol. 26, no. 2, pp. 23–37. DOI: 10.17212/1994-6309-2024-26.2-23-37. (In Russian).

## \* Corresponding author

Sirota Vyacheslav V., Ph.D. (Physics and Mathematics), Director  
Belgorod State Technological University named after V.G. Shukhov,  
46 Kostyukova st.,  
308012, Belgorod, Russian Federation  
Tel.: +7 904 539-14-08, e-mail: [zmas36@mail.ru](mailto:zmas36@mail.ru)

## Introduction

Ceramic composite materials have been actively used during the last decade for protection against abrasion and thermal corrosion. There have also been a number of works [1–6] devoted to the study of the emissivity of ceramic composite materials in order to use it as coatings on the heat-transferring surfaces of industrial furnaces to increase energy efficiency.

The heat treatment process is one of the most common technological operations in all industries. The heat energy transfer in the furnace occurs through convection and radiation mechanisms, but radiation heat transfer becomes dominant with increasing temperature [7]. The main criterion that characterizes the efficiency of radiation heat transfer is the emissivity of the heat-emitting surfaces, in industrial heating furnaces. Such surfaces are internal walls, gas ducts and coils, depending on the design and type of furnace.

Increasing the energy efficiency of industrial heating furnaces is currently considered as one of the promising ways to overcome the ever-growing energy crisis, because it is in heating processes that a large amount of energy is wasted [8]. To this end, ceramic composite coatings with high emissivity and thermal stability during operation consisting of powder compositions of  $Fe_2O_3$ ,  $Al_2O_3 + 10\% Fe_2O_3$ ,  $Ti + 10\% Fe_2O_3$  were developed and investigated. The effect of the presence of iron oxide and aluminum oxide in the coating on increasing emissivity was shown by other researchers [9–11]. Previously developed coatings were applied in different ways on the heat-transmitting walls of the furnace, which significantly improved the energy efficiency of heat energy transfer [9–12]. The emissivity coefficient of a material is the ability of its surface to radiate energy through radiative heat transfer; numerically this characteristic can be expressed as the ratio of the energy radiated by a particular material to the radiated energy of a absolutely black body at the same temperature, where a absolutely black body will have a value equal to 1, and for a comparable material the value is in the range from 0 to 1 [13].

At present, many methods have been studied for applying high-emissivity coatings to metal surfaces, for example: sol-gel method, glazing, magnetron sputtering, electron beam vapor deposition, plasma spraying, etc. [14–19]. In the presented work, the possibility of forming coatings with high emissivity coefficient on the heat-emitting surfaces of industrial baking ovens using detonation gas-dynamic spraying is investigated. This method makes it possible to apply coatings with low porosity (1 %) and high adhesion to the base [20], which will ensure the resistance of the coating to thermal cycling. The coating process is carried out by heating and accelerating powders by detonation combustion products of combustible gas mixture of propane, oxygen and air with a frequency of 20 Hz and above, the sprayed particles velocity using this method reaches 1,200 m/s, and the materials utilization rate for oxide ceramic powders is not less than 67 % [21, 22].

**The purpose of the work** is to obtain coatings with high emission indices in the infrared range for further recommendation of its use in baking ovens of *Shebekinsky* machine-building plant. To achieve the purpose the following tasks were solved:

1. The compositions were determined and powder compositions of  $Fe_2O_3$ ,  $Al_2O_3 + 10\% Fe_2O_3$ ,  $Ti + 10\% Fe_2O_3$  were prepared.
2. Technological parameters for applying powder compositions using the detonation gas-dynamic method were determined.
3. The structure and phase composition of the obtained coatings were investigated.
4. The emissivity of the obtained coatings was determined.
5. The thermal stability of the obtained coatings was studied.

## Research methodology

As raw components for the creation of coatings, powders *Ti* (*PTS-1*, purity 99 %),  $Al_2O_3$  (*ChDA*, purity 98.5 %),  $Fe_2O_3$  (extra-pure 2–4, purity 99.7 %) were purchased. The characteristics of the purchased powders are given in Table 1.

Mixing of powder compositions of  $Al_2O_3$ , *PTS-1* and  $Fe_2O_3$  was carried out mechanically in a *Fritsch Pulverisette 6* planetary mill at a mass ratio of balls to mixture of 2:1 at a speed of 200 rpm for 5 min.

Table 1

Powders used for coatings

Name, grade	Manufacturer	Method of obtaining	Particle size distribution, $\mu\text{m}$		
			$d(10)$	$d(50)$	$d(90)$
Ti powder, PTS-1	JSC POLEMA Tula, Russia	Amalgam metallurgy method	9.54	24.69	50.76
$\text{Al}_2\text{O}_3$ powder	Donetsk Chemical Reagents Plant	Initial material calcination in a halogen-containing atmosphere	2.28	19.96	46.36
$\text{Fe}_2\text{O}_3$ powder	Donetsk Chemical Reagents Plant	Utilization of thermal decomposition products of iron	0.23	5.54	27.9

Coating was carried out by detonation gas dynamic spraying using a robotic complex (Fig. 1) for detonation spraying of coatings, consisting of a multi-chamber shaped-detonation device (MCDS), a gas post, a gantry robot, and a special powder feeder, which provides dosing and periodic powder feeding into the MCDS. Powder injection into the combustion chamber of the MCDS in the process of detonation of the combustible gas mixture ensures its heating and acceleration. Heated powders hit the substrate surface at high speed, creating a dense composite coating [23–25].

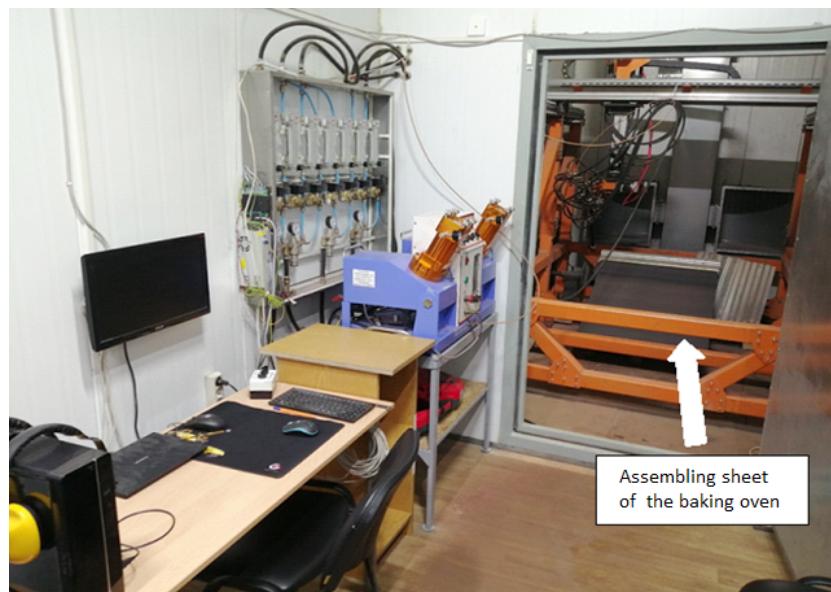


Fig. 1. Robotic complex for detonation coating

The right side of Figure 1 shows the assembling sheet of the coated baking oven. After coating all the heat-transferring surfaces of the oven components, the baking chamber is assembled.

The baking chambers in the baking ovens of the *Shebekinsky Machine-Building Plant* are made of St3 steel. The finished baking oven of the *Shebekinsky Machine-Building Plant* is shown in Figure 2.

A series of experimental specimens of coatings on a substrate of St3 steel with dimensions of 40×40 mm (3 specimens for each coating material) were fabricated to study the microstructure, phase composition, resistance to thermal cycling and emissivity.

Before coating, the surface of experimental specimens was cleaned from oil contamination with hexane and subjected to sandblasting. Sandblasting was carried out at a pressure of 0.3 MPa with dry quartz sand with grain size 1–3 mm up to the 3<sup>rd</sup> class of purity according to GOST 9.402-82. Afterwards, residual

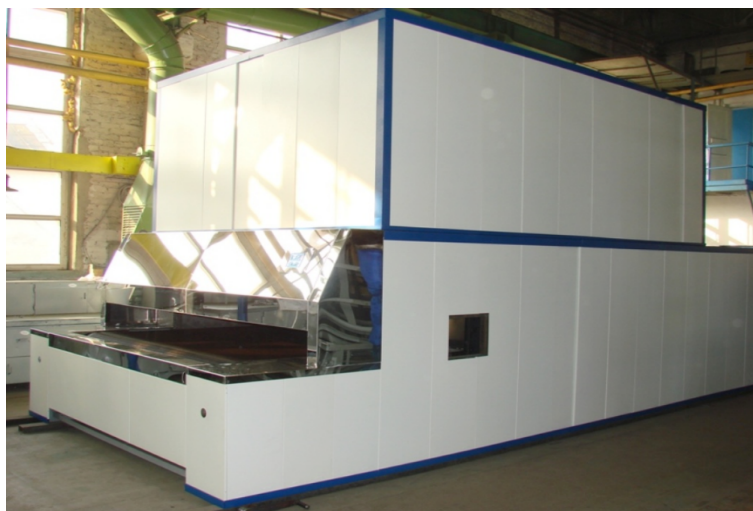


Fig. 2. Appearance of a baking oven of JSC SHMZ

contamination was removed from the surface of the metal plate by compressed air not worse than the 1<sup>st</sup> class of contamination according to *GOST 17433*.

The modes of coating on the surface of the experimental specimens are given in Table 2.

Table 2

Coating parameters

Powder name	Flow rate of fuel mixture components (m <sup>3</sup> /h)			Powder consumption (g/h)	Spraying distance (mm)
	air	oxygen	propane (30 %) + butane (70 %)		
$Fe_2O_3$	1.41*/1.08**	2.87*/3.26**	0.54*/0.65**	11	40
$Al_2O_3 + 10 \% Fe_2O_3$	1.41*/1.08**	2.87*/3.26**	0.54*/0.65**	52	70
$Ti + 10 \% Fe_2O_3$	1.3*/1.54**	2.44*/3.04**	0.56*/0.67**	78	65
* – cylindrical combustion chamber; ** – annular combustion chamber/					

The coating was applied by moving the barrel in the vertical scanning mode with a transverse displacement of 5 mm in one pass. The inner diameter of the barrel was 16 mm, the barrel length was 500 mm, and the detonation frequency was 20 Hz. The barrel displacement in vertical scanning mode for  $Fe_2O_3$ ,  $Al_2O_3 + 10 \% Fe_2O_3$  and  $Ti + 10 \% Fe_2O_3$  composite coatings was carried out at a speed of 2,000 mm/min, 1,000 mm/min, 1,500 mm/min, respectively.

To determine the microstructure and phase composition, the obtained experimental specimens were sawn into 4 parts with dimensions of 20×20 mm using an *IsoMet 5000* precision cutting machine.

The microstructure, elemental composition and morphology of the obtained coatings were investigated by scanning electron microscopy on a scanning electron microscope *Mira 3 LMU* (*Tescan*, Czech Republic). A reflected electron detector was used in high-resolution mode at an accelerating voltage of 15 kV to obtain images of the surface of composite coatings and areas for the study of the elemental composition. The elemental composition of the specimens was studied by energy dispersive spectroscopy (*EDS*) in the *AZtec 3.1* microanalysis system using an *X-Max 50* detector (*Oxford Instruments NanoAnalysis*, High Wycombe, England). The accumulation of *EDS* spectra and elemental composition distribution maps was carried out at an accelerating voltage of 15 kV, working distance 15 mm. The beam current was set so that the signal level was about 4,000–5,000 pulses per second.



The phase composition of the coated experimental specimens was analyzed by X-ray diffraction with stepwise scanning of  $2\theta$  angles from  $10$  to  $90^\circ$  with a step of  $0.05^\circ$  on an *ARL X'TRA* diffractometer (*Thermo Fisher Scientific*, Switzerland) with *Cu-K $\alpha$* -radiation ( $\lambda = 0.1541744$  nm). The phase composition was determined according to the standard technique in the *PDXL* program using the *PDF-2 (JCPDS ICDD)* powder radiographic standards database (2008).

The infrared spectra were measured on an *IRS 55/S IR* Fourier spectrometer (*Bruker*, Germany) using a registration monochromator controlled by a personal computer (*PC*). Diffraction gratings of 300 and 150 shp/mm were used to extend the spectral range. The working spectral range of the gratings was  $1.4\text{--}4.0$  and  $2.8\text{--}8.0$   $\mu\text{m}$ , respectively. Measurements were performed at a spectral slit width of  $0.02$   $\mu\text{m}$ . The scanning step was chosen to be  $10$  nm. Due to the high absorption capacity of quartz lenses designed to focus radiation to the input slit of the monochromator in the range from  $2.5$   $\mu\text{m}$ , the latter were removed and replaced by mirrors. The distance from the heated specimen (coated plate) to the monochromator slit was  $60$  cm. The focused radiation from the specimens was fed to the input slit of the monochromator using an aluminum mirror with focal length  $f = 150$  mm. Mirror adapters (elliptical aluminum reflectors) were used behind the output slit of the monochromator, the use of which made it possible to collect the output radiation from the monochromator to the receiving area of the photodetector with minimal losses.

In the  $1.0\text{--}4.0$   $\mu\text{m}$  range, an automated turret with interference *IR* light filters switchable at wavelengths of  $1.0$ ,  $1.6$ , and  $2.0$   $\mu\text{m}$  was used to cut off higher-order radiation. In the  $4.0\text{--}8.0$   $\mu\text{m}$  range, additional manually switchable *IR* light filters were used for a similar purpose. In the extended range of  $1.0\text{--}10.0$   $\mu\text{m}$ , a module from *Oriel Instruments* (USA) was used as a photodetector (detector), the sensitivity of which did not depend on the radiation wavelength.

During preliminary adjustment (debugging) of the recording system (signal search and optimization) in the near-infrared range ( $1.0\text{--}2.0$   $\mu\text{m}$ ) we used more highly sensitive detectors: *InGaAs*-photodiodes *IGA-050-TE2-H* ( $900\text{--}1,700$  nm), *IGA2.2-030-TE2-H* ( $900\text{--}2,800$  nm) and *PbS*-photoresistors *PbS-050-TE2-H*, ( $900\text{--}3,300$  nm) of the company "*ELECTRO-OPTICAL SYSTEMS INC*" (USA-Canada); *InGaAsP* photodiodes *PD24-20TEC1-PR* ( $1,000\text{--}2,300$  nm), *PD25-20TEC1-PR* ( $1,000\text{--}2,500$  nm), *PD36-05PR* ( $1,200\text{--}3,800$  nm) of the company "*IBSG Company Ltd*" (St. Petersburg, Russia). The photodiodes and photoresistors were cooled to optimal temperatures. To increase the signal-to-noise ratio, registration was performed using radiation modulation at the input of the monochromator. The modulation frequency was  $500$  Hz. The pre-amplified signal from the detectors was fed to the main single-channel amplifier with a synchronous detector Lock-in nanovoltmeter type 232 B (Poland, USA).

For spectral measurements of specimens in the temperature range from  $100$  to  $500$   $^\circ\text{C}$ , a method was developed and a thermoblock (mini oven) with heating of specimens and maintenance of its temperature (relative to the required temperature) with an error of  $\pm 5$   $^\circ\text{C}$ . The thermoblock consists of a heater, a heat conducting sleeve made of copper ( $d = 40$  mm, thickness  $h = 8$  mm) and a heat-resistant casing. A  $20 \times 20$  mm specimen was pressed to the copper sleeve using screws. Temperature control was carried out using a calibrated constantan-copper thermocouple inserted into the hole of the copper sleeve. The required specimen temperature was maintained by selecting the heater current.

The error in spectra measurements in the vast majority of cases did not exceed  $\pm 5$  %. In some cases, when the useful signal exceeded the background (noise) signal only  $5\text{--}10$  times, the error could reach  $\pm 10$  %.

Thermal cycling of coated specimens was carried out in a muffle furnace. For each test, three specimens were placed on a tray. The tray could be moved in and out of the furnace chamber. An air-cooling system was attached to the outside of the chamber to cool the specimens. The oven temperature was set at  $550$   $^\circ\text{C}$ , as this is the maximum operating temperature of the hottest parts of the heat transfer surfaces of the baking oven. The specimens were kept in the muffle oven for  $30$  min. Then the moving tray with the specimens was removed from the oven and air cooling was applied to the for  $10$  min. One thermal cycle consisted of  $30$  min heating and  $10$  min air cooling. The specimens underwent  $300$  cycles to evaluate the effect on the coating.

## Results and their discussion

The initial powders are represented by a wide range of particles of different shapes, among which we can distinguish splinter, spongy, droplet, as well as particles of complex shape. The results of the study of morphology and particle size of the initial powders are shown in Figure 3.

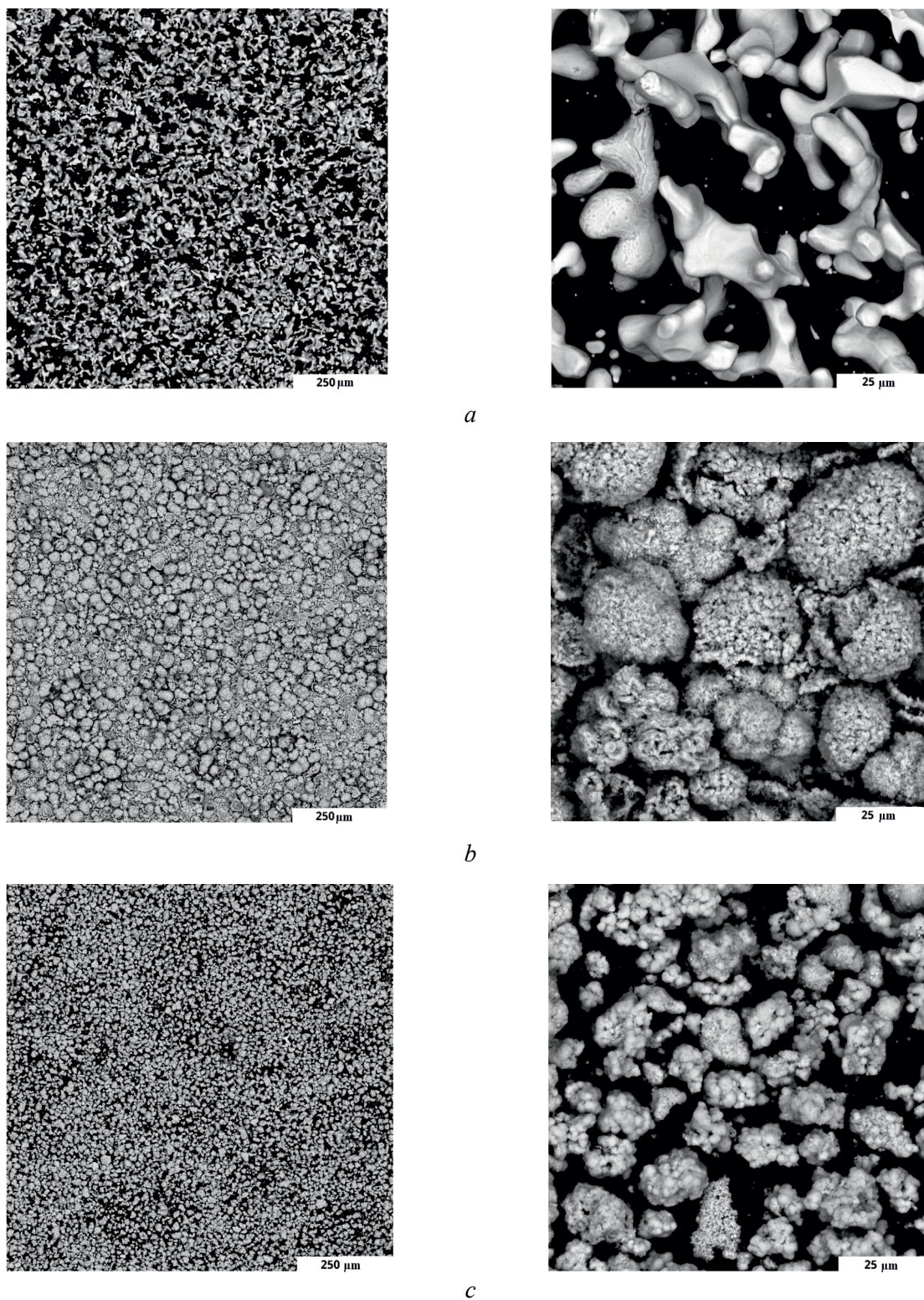


Fig. 3. Morphology and particle size of the initial powders:  
*PTS-1 (a),  $Al_2O_3$  (b),  $Fe_2O_3$  (c)*



The results of the study of the phase composition of the initial powders are summarized in Table 3.

The results of the study of the particle size distribution of the initial powders are summarized in Table 4.

Figure 4 shows the SEM images of the experimental coating specimens sections.

A 5  $\mu\text{m}$  thick coating of  $\text{Fe}_2\text{O}_3$  powder was formed on *St3* steel (Figure 4, *a*). The contact zone between the coating and the substrate has no defects or microcracks, which indicates high strength of the joint.

The coating applied from a composition of  $\text{Al}_2\text{O}_3 + 10\% \text{Fe}_2\text{O}_3$  powders (Figure 4, *b*) is continuous, without chipping, bubbles and through cracks. The thickness of the obtained coating is 50  $\mu\text{m}$ .

When studying the structure of the coating formed from the composition of powders  $\text{Ti} + 10\% \text{Fe}_2\text{O}_3$  (Fig. 4, *c*), it was found that it has a developed lamellar structure with a large number of interphase boundaries. The coating is dense, there are no cracks and pores, and the coating thickness is 5  $\mu\text{m}$ .

The results of energy dispersive spectroscopy are summarized in Table 5.

Table 3

## Phase composition of the initial powders

Name, grade	Phase	Spatial group
PTS-1 powder	Ti	194:P63/mmc
Powder PDA $\text{Al}_2\text{O}_3$	$\gamma\text{-Al}_2\text{O}_3$	227:Fd3m
Powder extra-pure 2-4 $\text{Fe}_2\text{O}_3$	$\alpha\text{-Fe}_2\text{O}_3$	167:R-3c

Table 4

## Granulometric composition of the initial powders

Name, grade	Particle size distribution, $\mu\text{m}$		
	$d(10)$	$d(50)$	$d(90)$
<i>Ti</i> powder, <i>PTS-1</i>	9.54	24.69	50.76
Powder $\text{Al}_2\text{O}_3$	2.28	19.96	46.36
Powder $\text{Fe}_2\text{O}_3$	0.23	5.54	27.9

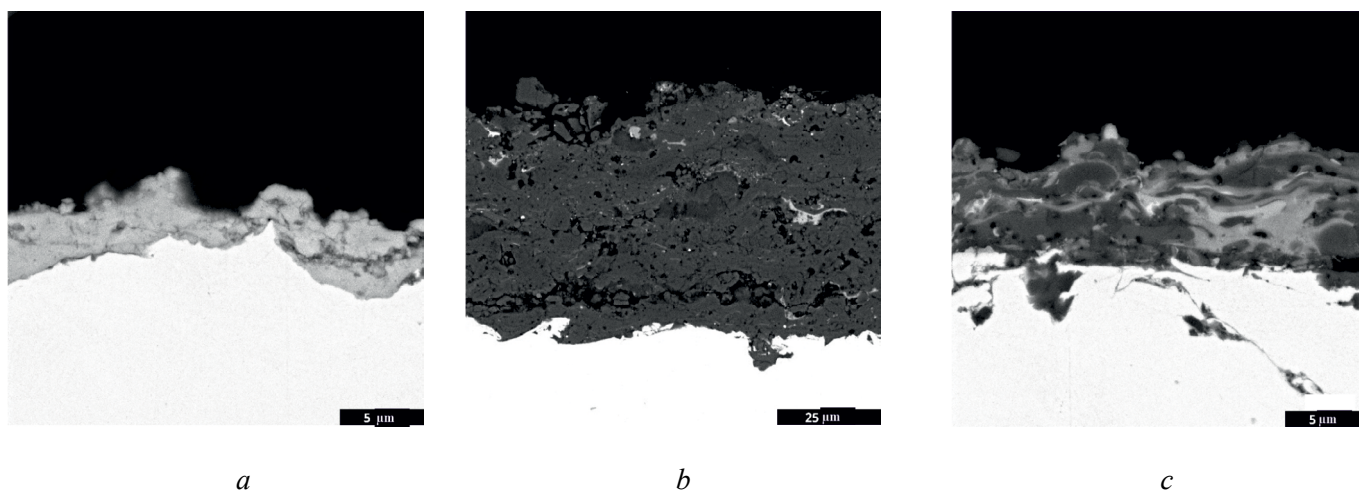


Fig. 4. Microstructure and morphology of the cross-section surface of experimental coating samples:

$\text{Fe}_2\text{O}_3$  (*a*),  $\text{Al}_2\text{O}_3 + 10\% \text{Fe}_2\text{O}_3$  (*b*),  $\text{Ti} + 10\% \text{Fe}_2\text{O}_3$  (*c*)

Table 5

## Results of energy-dispersive spectroscopy

Coverage	Element, weight %			
	<i>O</i>	<i>Al</i>	<i>Ti</i>	<i>Fe</i>
$Fe_2O_3$	30.1	–	–	69.9
$Al_2O_3 + 10\% Fe_2O_3$	45.7	49.2	–	5.1
$Ti + 10\% Fe_2O_3$	39.6	–	54.1	6.3

The results of energy dispersive spectroscopy (EDS), confirmed the expected elemental composition of the witness specimens. The composition corresponds to the composition of the initial powders.

The results of the study of the phase composition of the coatings are summarized in Table 6.

Table 6

## Phase of composite coatings

Coverage	Phase	Spatial group	Composition, %
$Fe_2O_3$	$Fe_3O_4$	74:Imma	100
$Al_2O_3 + 10\% Fe_2O_3$	$\alpha-Al_2O_3$	167:R-3c	54
	$\gamma-Al_2O_3$	227:Fd3m	39
	$Fe_3O_4$	227:Fd-3m	7
$Ti + 10\% Fe_2O_3$	$TiO_2$	136:P42/mnm	91
	$Fe_3O_4$	227:Fd-3m	9

When coating from a composition of  $Al_2O_3 + 10\% Fe_2O_3$  powders, a structure consisting of  $\alpha-Al_2O_3$ ,  $\gamma-Al_2O_3$  and  $Fe_3O_4$  solid solution phases is formed.

The coating obtained from the composition of powders  $Ti + 10\% Fe_2O_3$  consists of phases  $TiO_2$  and  $Fe_3O_4$ . The transition of the  $Ti$  phase into the  $TiO_2$  phase is due to the oxidation of titanium, which occurs during the formation of the coating.

Figure 5 shows the results of measuring the emissivity of experimental specimens of coatings at 450 °C. The dips in the region of 4.25  $\mu m$  are caused by absorption of carbon dioxide, in the region of 1.82, 3.3, 5.9 and 6.5  $\mu m$  are caused by steam.

Among the experimental specimens obtained, the coating  $Fe_2O_3$  at 450 °C showed the highest emissivity in the infrared range  $\epsilon_{3-7} \mu m = 0.7$  and  $\epsilon_{4-5} \mu m = 0.8$ . Composite coatings of  $Al_2O_3 + 10\% Fe_2O_3$  and  $Ti + 10\% Fe_2O_3$  have  $\epsilon_{3-7} \mu m = 0.59$  and 0.57, respectively, and  $\epsilon_{4-5} \mu m = 0.67$  and 0.66 at 450 °C. Coating  $Fe_2O_3$  has the main peak of IR radiation in the region of 3–4  $\mu m$ , which is more promising for use in the baking industry, because the radiation of this spectral range most deeply penetrates into the dough, accelerating the cooking process.

According to the results of the analysis of the results of thermal cycling of experimental specimens, it was revealed that the appearance of coatings did not change. The appearance of the coating specimens after thermal cycling is shown in Figure 6.

The specimens underwent 300 cycles of thermal cycling without cracks and delaminations. The analysis of X-ray phase diagram showed that after thermocycling there were no changes in the crystal lattice, which indicates a high resistance of coatings to operational temperature changes. The results are presented in Figure 7.



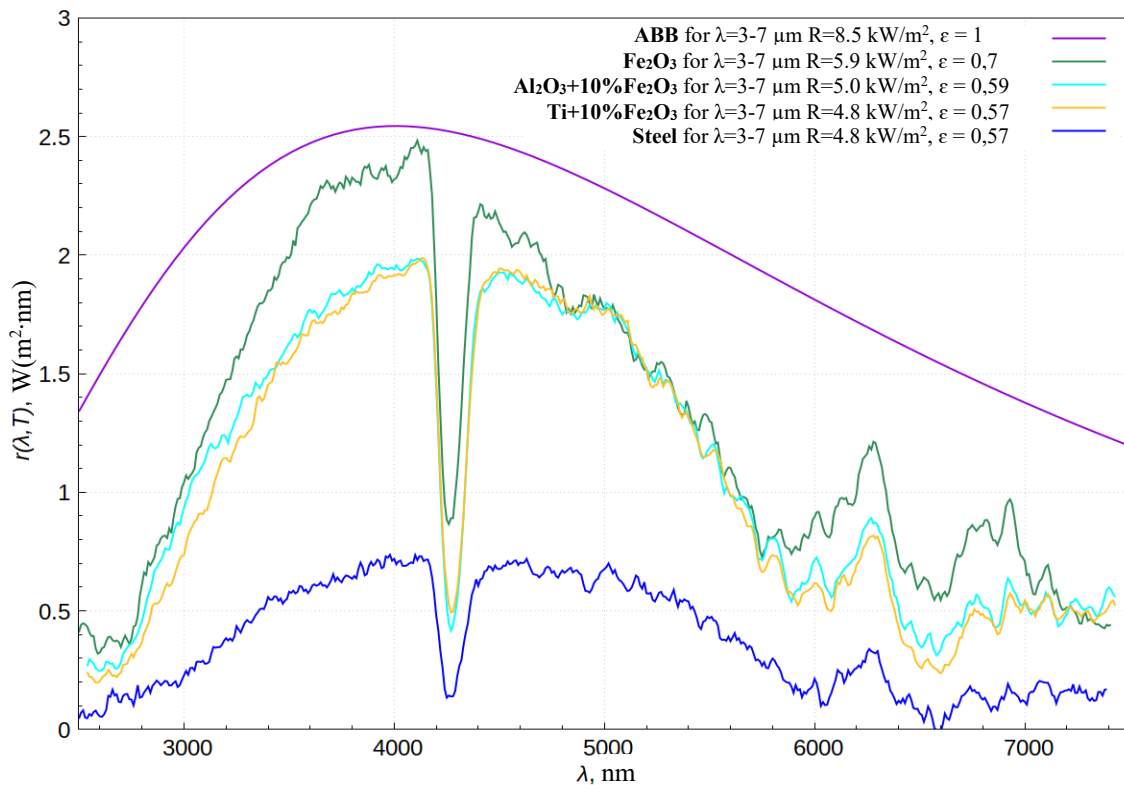


Fig. 5. Spectral emissivity of experimental coating samples at 450°C

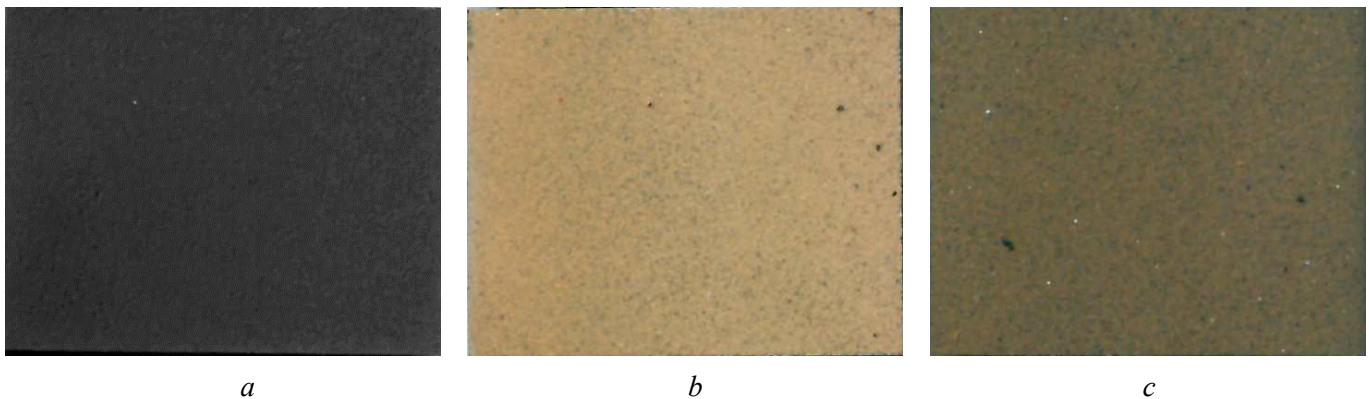


Fig. 6. Appearance of coating samples after thermal cycling:

$\text{Fe}_2\text{O}_3$  (a);  $\text{Al}_2\text{O}_3 + 10 \% \text{Fe}_2\text{O}_3$  (b);  $\text{Ti} + 10 \% \text{Fe}_2\text{O}_3$  (c)

## Conclusions

Coatings  $\text{Fe}_2\text{O}_3$ ;  $\text{Al}_2\text{O}_3 + 10 \% \text{Fe}_2\text{O}_3$ ,  $\text{Ti} + 10 \% \text{Fe}_2\text{O}_3$ , obtained by detonation gas dynamic powder spraying were studied for JSC Shebekino Machine Building Plant, Shebekino.

Analysis of the microstructure of the obtained coatings showed that it has a dense lamellar structure with the absence of cracks.

The results of high-temperature cyclic heat treatment showed that the obtained coatings are resistant to operating temperatures.

X-ray diffraction analysis showed that no changes in the crystal lattice of the coatings occurred under the influence of cyclic heat treatment.

The results of infrared spectrometry of the obtained coatings show that at  $T = 450^\circ\text{C}$  about 5 kW of power can be obtained per square meter of a coating with a high emission coefficient. According to the

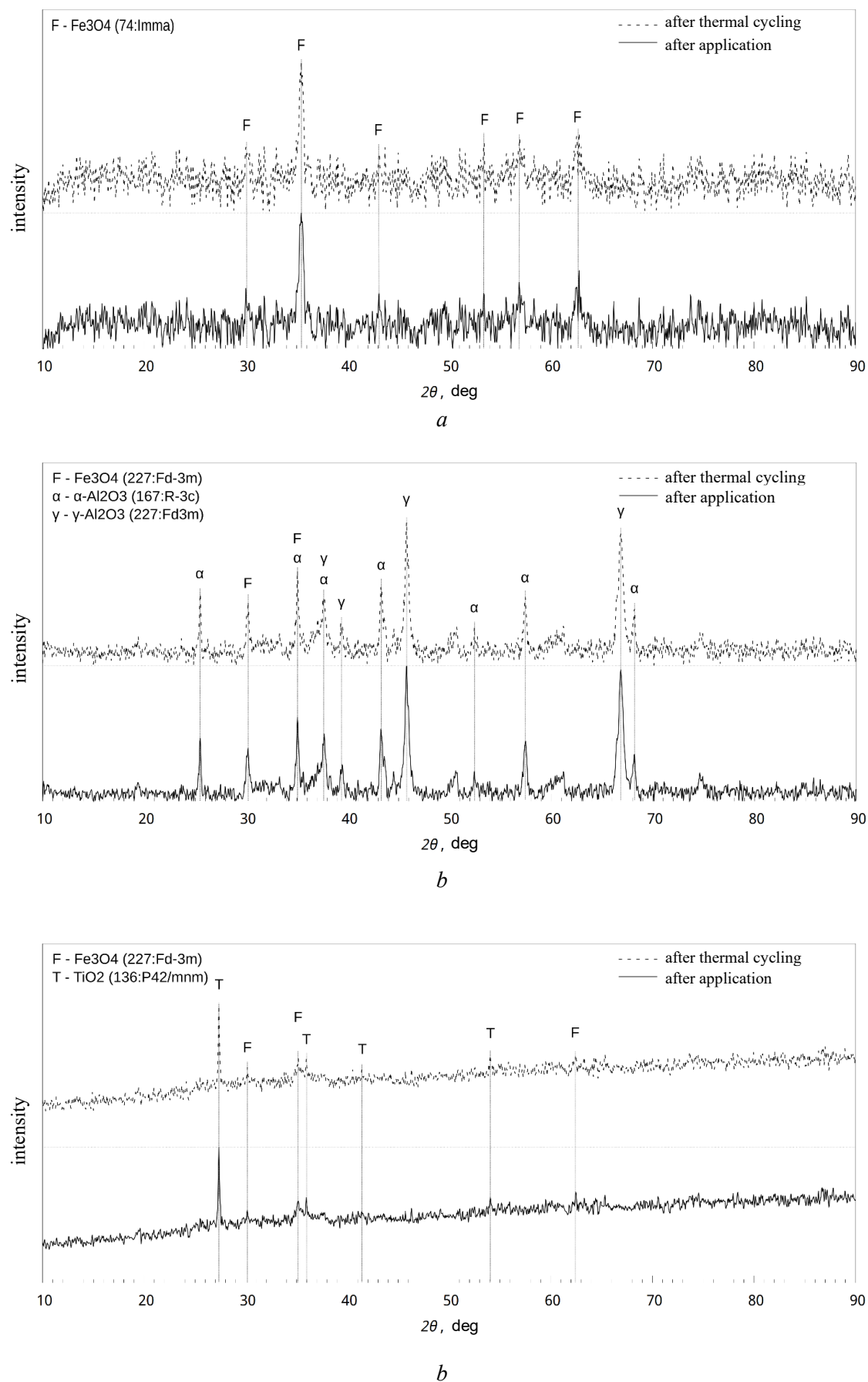


Fig. 7. Comparison of the results of X-ray phase analysis before and after thermal cycling:

$Fe_2O_3$  (a);  $Al_2O_3 + 10\% Fe_2O_3$  (b);  $Ti + 10\% Fe_2O_3$  (c)



technical characteristics of baking ovens produced by *Shebekinsky machine-building plant*, the estimated average power is 1 kW per square meter of a coating. Thus, the obtained specimens with coatings  $Fe_2O_3$ ;  $Al_2O_3 + 10\% Fe_2O_3$ ;  $Ti + 10\% Fe_2O_3$  give the supplied energy at 450 °C more than 3 times more efficient than the specimens of steel *St3*, from which the ovens are made. Theoretically, even at 200 °C, more than 1 kW/m<sup>2</sup> can be removed from the coating.

## References

1. Tan W., Petorak C.A., Trice R.W. Rare-earth modified zirconium diboride high emissivity coatings for hypersonic applications. *Journal of the European Ceramic Society*, 2014, vol. 34 (1), pp. 1–11. DOI: 10.1016/j.jeurceramsoc.2013.07.016.
2. Tang H., Xin T., Sun Q., Yi C., Jiang Z., Wang F. Influence of  $FeSO_4$  concentration on thermal emissivity of coatings formed on titanium alloy by micro-arc oxidation. *Applied Surface Science*, 2011, vol. 257 (24), pp. 10839–10844. DOI: 10.1016/j.apsusc.2011.07.118.
3. Li X., Peoples J., Yao P., Ruan X. Ultrawhite  $BaSO_4$  paints and films for remarkable daytime subambient radiative cooling. *ACS Applied Materials & Interfaces*, 2021, vol. 13 (18), pp. 21733–21739. DOI: 10.1021/acsami.1c02368.
4. Liu J., Chen Z., Yang L., Chai P., Wan Q. The effect of SiC coatings microstructure on their infrared emissivity. *Journal of Asian Ceramic Societies*, 2023, vol. 11 (1), pp. 98–104. DOI: 10.1080/21870764.2022.2159952.
5. Shao G., Wu X., Cui S., Shen X., Kong Y., Lu Y., Jiao C., Jiao J. High emissivity  $MoSi_2$ - $ZrO_2$ -borosilicate glass multiphase coating with  $SiB_6$  addition for fibrous  $ZrO_2$  ceramic. *Ceramics International*, 2016, vol. 42 (7), pp. 8140–8150. DOI: 10.1016/j.ceramint.2016.02.020.
6. Huang X., Li N., Wang J., Liu D., Xu J., Zhang Z., Zhong M. Single nanoporous  $MgHPO_4 \cdot 1.2H_2O$  for daytime radiative cooling. *ACS Applied Materials & Interfaces*, 2019, vol. 12 (2), pp. 2252–2258. DOI: 10.1021/acsami.9b14615.
7. Švantner M., Honnerová P., Veselý Z. The influence of furnace wall emissivity on steel charge heating. *Infrared Physics & Technology*, 2016, vol. 74, pp. 63–71. DOI: 10.1016/j.infrared.2015.12.001.
8. Zhao J., Ma L., Zayed M.E., Elsheikh A.H., Li W., Yan Q., Wang J. Industrial reheating furnaces: A review of energy efficiency assessments, waste heat recovery potentials, heating process characteristics and perspectives for steel industry. *Process Safety and Environmental Protection*, 2021, vol. 147, pp. 1209–1228. DOI: 10.1016/j.psep.2021.01.045.
9. Sako E.Y., Orsolini H.D., Moreira M., De Sousa Meneses D., Pandolfelli V.C. Emissivity of spinel and titanate structures aiming at the development of industrial high-temperature ceramic coatings. *Journal of the European Ceramic Society*, 2021, vol. 41 (4), pp. 2958–2967. DOI: 10.1016/j.jeurceramsoc.2020.11.010.
10. Mahadik D.B., Gujjar S., Gouda G.M., Barshilia H.C. Double layer  $SiO_2/Al_2O_3$  high emissivity coatings on stainless steel substrates using simple spray deposition system. *Applied Surface Science*, 2014, vol. 299, pp. 6–11. DOI: 10.1016/j.apsusc.2014.01.159.
11. Gahmouss A., Ferria K., Rubio J., Cornejo N., Tamayo A. Influence of  $Fe_2O_3$  on the structure and near-infrared emissivity of aluminosilicate glass coatings. *Applied Physics A*, 2020, vol. 126 (9), p. 732. DOI: 10.1007/s00339-020-03921-8.
12. Heynderickx G.J., Nozawa M. High-emissivity coatings on reactor tubes and furnace walls in steam cracking furnaces. *Chemical Engineering Science*, 2004, vol. 59 (22–23), pp. 5657–5662. DOI: 10.1016/j.ces.2004.07.075.
13. Mauer M., Kalenda P., Honner M., Vacikova P. Composite fillers and their influence on emissivity. *Journal of Physics and Chemistry of Solids*, 2012, vol. 73 (12), pp. 1550–1555. DOI: 10.1016/j.jpcs.2011.11.015.
14. He B., Li F., Zhou H., Dai Y., Sun B. Study of failure of EB-PVD thermal barrier coating upon near- $\alpha$  titanium alloy. *Journal of Materials Science*, 2008, vol. 43, pp. 839–846. DOI: 10.1007/s10853-007-2204-7.
15. Zukerman I., Zhitomirsky V.N., Beit-Ya'akov G., Boxman R.L., Raveh A., Kim S.K. Vacuum arc deposition of  $Al_2O_3$ - $ZrO_2$  coatings: arc behavior and coating characteristics. *Journal of Materials Science*, 2010, vol. 45, pp. 6379–6388. DOI: 10.1007/s10853-010-4734-7.
16. Shin D.-I., Gitzhofer F., Moreau C. Thermal property evolution of metal based thermal barrier coatings with heat treatments. *Journal of Materials Science*, 2007, vol. 42, pp. 5915–5923. DOI: 10.1007/s10853-007-1772-x.
17. Tang H., Sun Q., Yi C.G., Jiang Z.H., Wang F.P. High emissivity coatings on titanium alloy prepared by micro-arc oxidation for high temperature application. *Journal of Materials Science*, 2012, vol. 47, pp. 2162–2168. DOI: 10.1007/s10853-011-6017-3.





18. Zhang H., Wang C., Wang Y., Wang S., Chen G., Zou Y., Deng C., Jia D., Zhou Y. Ca-Mn co-doping  $\text{LaCrO}_3$  coating with high emissivity and good mechanical property for enhancing high-temperature radiant heat dissipation. *Journal of the European Ceramic Society*, 2022, vol. 42 (15), pp. 7288–7299. DOI: 10.1016/j.jeurceramsoc.2022.08.033.

19. Yao Z., Hu B., Shen Q., Niu A., Jiang Z., Su P., Ju P. Preparation of black high absorbance and high emissivity thermal control coating on Ti alloy by plasma electrolytic oxidation. *Surface and Coatings Technology*, 2014, vol. 253, pp. 166–170. DOI: 10.1016/j.surfcoat.2014.05.032.

20. Kolisnichenko O.V., Tyurin Yu.N., Tovbin R. Effektivnost' protsessy napyleniya pokrytii s ispol'zovaniem mnogokamernogo detonatsionnogo ustroystva [Efficiency of process of coating spraying using multi-chamber detonation unit]. *Avtomaticeskaya svarka = The Paton Welding Journal*, 2017, no. 10, pp. 28–34.

21. Kovaleva M., Prozorova M., Arsenko M., Tyurin Y., Kolisnichenko O., Yapryntsev M., Novikov V., Vagina O., Sirota V. Zircon-based ceramic coatings formed by a new multi-chamber gas-dynamic accelerator. *Coatings*, 2017, vol. 7 (9), p. 142. DOI: 10.3390/coatings7090142.

22. Sirota V.V., Zaitsev S., Prokhorenkov D., Limarenko M., Skiba A., Kovaleva M.G. Detonation spraying of composite targets based on Ni, Cr and  $\text{B}_4\text{C}$  for magnetron multi-functional coating. *Key Engineering Materials*, 2022, vol. 909, pp. 115–120. DOI: 10.4028/p-74w31h.

23. Kovaleva M., Goncharov I., Novikov V., Yapryntsev M., Vagina O., Pavlenko I., Sirota V., Tyurin Y., Kolisnichenko O. Effect of heat treatment on the microstructure and phase composition of  $\text{ZrB}_2\text{-MoSi}_2$  coating. *Coatings*, 2019, vol. 9 (12), p. 779. DOI: 10.3390/coatings9120779.

24. Wang Q., Sun Q., Zhang M.-X., Niu W.-J., Tang C.-B., Wang K.-S., Xing R., Zhai L., Wang L. The influence of cold and detonation thermal spraying processes on the microstructure and properties of Al-based composite coatings on Mg alloy. *Surface and Coatings Technology*, 2018, vol. 352, pp. 627–633. DOI: 10.1016/j.surfcoat.2018.08.045.

25. Endo T., Obayashi R., Tajiri T., Kimura K., Morohashi Y., Johzaki T., Matsuoka K., Hanafusa T., Mizunari S. Thermal spray using a high-frequency pulse detonation combustor operated in the liquid-purge mode. *Journal of Thermal Spray Technology*, 2016, vol. 25, pp. 494–508. DOI: 10.1007/s11666-015-0354-8.

## Conflicts of Interest

The authors declare no conflict of interest.

© 2024 The Authors. Published by Novosibirsk State Technical University. This is an open access article under the CC BY license (<http://creativecommons.org/licenses/by/4.0>).